Journal of Molecular Structure 1157 (2018) 165–176

Contents lists available at ScienceDirect

Journal of Molecular Structure

journal homepage: http://www.elsevier.com/locate/molstruc

Synthesis, spectroscopic characterization and a comparative study of the corrosion inhibitive efficiency of an α-aminophosphonate and Schiff base derivatives: Experimental and theoretical investigations

Khalissa Benbouguerra [a, b, *], Salah Chafaa [a], Nadjib Chafai [a], Mouna Mehri [a], Ouahiba Moumeni [a], Abdelkader Hellal [a]

[a] Laboratory of Electrochemical Molecular Materials and Complex LEMMC, Department of Process Engineering, Faculty of Technology, El-Maabouda, University Ferhat ABBAS Setif -1, 19000 Setif, Algeria
[b] Department of Chemistry, Faculty of Sciences, El-Baz, University Ferhat ABBAS Setif -1, 19000 Setif, Algeria

ARTICLE INFO

Article history:
Received 31 August 2017
Received in revised form
13 December 2017
Accepted 13 December 2017
Available online 16 December 2017

Keywords:
α-aminophosphonate
Schiff base
Corrosion inhibition
Quantum chemical calculations
Molecular dynamics simulations

ABSTRACT

New α-aminophosphonate (**α-APD**) and Schiff base (**E-NDPIMA**) derivatives have been prepared and their structures ware proved by IR, UV–Vis, ^{1}H, ^{13}C and ^{31}P NMR spectroscopy. Their inhibitive capacities on the XC48 carbon steel corrosion in 0.5 mol L^{-1} H_2SO_4 solution were explored by weight loss, Tafel polarization, electrochemical impedance spectroscopy (EIS) and atomic force microscope (AFM). Experimental results illustrate that the synthesized compounds are an effectives inhibitors and the adsorption of inhibitors molecules on the carbon steel surface obeys Langmuir adsorption isotherm. In addition, quantum chemical calculations performed with density function theory (DFT) method have been used to correlate the inhibition efficiency established experimentally. Also, the molecular dynamics simulations have been utilized to simulate the interactions between the inhibitors molecules and Fe (100) surface in aqueous solution.

1. Introduction

Corrosion of steel is a major problem in our daily lives and in various industrial plants. In this context, many techniques and methods have been developed and used to protect steel against corrosion. However, in practice, the most employed technique is the use of organic inhibitors and it has a great importance and applications in the protection of metals and alloys. Many studies have been conducted to determine the inhibition activity in aqueous solutions of several synthesized organic compounds [1–6].

α-aminophosphonate and Schiff bases derivatives have been attracting an outstanding attention during the last decade as a promising class of viable compounds in the corrosion inhibition field. The aromatic α-aminophosphonates and Schiff bases containing nitrogen, oxygen and sulfur atoms in their structure are also very attractive inhibition agents [7–10]. In the literature, many α-aminophosphonate and Schiff bases have announced as powerful corrosion inhibitors for various metals and alloys in acidic mediums [11–14]. Many synthetic methods for the synthesis of this type of compounds have been developed during the past years [15–19]. Of these methods, the Kabachnik-Field's [20–23] synthesis of α-aminophosphonates, promoted by acidic or basic catalysts, is the most appropriate.

Many reviews have been recently reported considering the employ of quantum chemical methods and molecular dynamic simulations techniques in corrosion inhibitor studies [24–26]. A number of investigators inform that the protecting activity of an inhibitor generally relies on several physicochemical and electronic properties of the protective molecules, especially, its organic functional groups, steric properties, electronic density of contributor atoms, and orbital characteristic of sharing electrons [27,28]. The great importance of the molecular dynamic simulations is the understanding of the fixation manner of inhibitor molecules on metal surface at molecular level and permits determining the adsorption energy value [29,30].

In the present study, we detail the preparation and characterization of two new α-aminophosphonate **α-APD** and Schiff base **E-**

* Corresponding author. Laboratory of Electrochemical Molecular Materials and Complex LEMMC, Department of Process Engineering, Faculty of Technology, El-Maabouda, University Ferhat ABBAS Setif -1, 19000 Setif, Algeria.
E-mail address: kh.benbouguerra@gmail.com (K. Benbouguerra).

https://doi.org/10.1016/j.molstruc.2017.12.049
0022-2860/

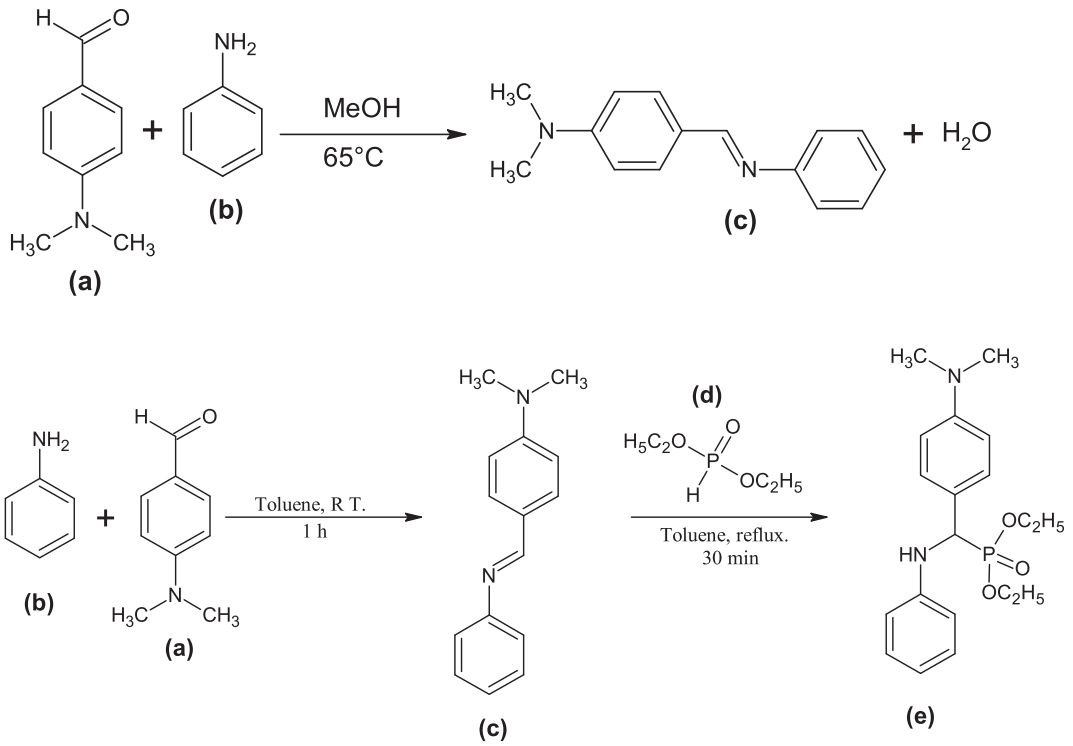

Fig. 1. Synthesis route of the studied compounds:**(a)** 4-(dimethylamino)benzaldehyd **(b)** Aniline **(c)** (E)-N, N-dimethyl-4-((phenylimino) methyl) aniline (**E-NDPIMA**) **(d)** diethylphosphite **(e)** diethyl ((4-(dimethylamino)phenyl)(phenylamino)methyl)phosphonate (**α-APD**).

NDPIMA derivatives. We also report a discussion of carbon steel XC48 corrosion in sulfuric acid medium by means of gravimetric tests, potentiodynamic polarization curves and electrochemical impedance spectroscopy (EIS). The adsorption isotherm of the inhibitors molecules on carbon steel surface and the thermodynamics parameters were obtained. On the other hand, the surface state of the carbon steel specimens was observed by employing atomic force microscopy (AFM). Besides, quantum chemical computations were applied to correlate experimental results. Finally, molecular dynamic simulations studies were performed to determinate the fixation forms and energies of the studied inhibitors on the iron face.

2. Experimental and theoretical layouts

2.1. Material, steel specimens, electrodes and solutions

All essays were realized on XC48 carbon steel of the corresponding chemical composition: (C = 0.418%, Mn = 0.730%, Mo = 0.012%, P = .016%, S = 0.019%, Si = 0.245%, Ni = 0.079%, F = 0.777% and Fe = 98.09873%). The carbon steel samples applied in weight loss measurements are sectioned to cylindrical samples of 9.42 cm^2 area. The working electrode employed in electrochemical measurements has a cylindrical form of 1.131 cm^2 frontal area prepared from rod XC48 carbon steel and soldered in the opposite area with Copper cable for an electrical connection. In the other hand, the side surface of the working electrode is installed on a plastic support to present only one active plane face displayed to the corrosive medium. The all metallic samples were mechanically polished on SiC papers of grades (600, 800, 1000, 1200, 1800 and 2500) and rinsed with distilled water. The analytical grade of 98% H_2SO_4 is used to obtain the 0.5 mol L^{-1} H_2SO_4 solutions by dilution with distilled water and varying amounts of the investigated derivatives were dissolved in 0.5 mol L^{-1} H_2SO_4 to prepare various concentrations of inhibitors solutions.

2.2. Preparation of the studied inhibitors

2.2.1. Preparation of the Schiff base derivative

The studied Schiff base derivative; namely (E)-N,N-dimethyl-4-((phenylimino)methyl)aniline (**E-NDPIMA**), was synthesized by condensation of 1.0 mmol of aniline with 1.0 mmol of 4-(dimethylamino)benzaldehyde in methanol at 65 °C. After a few hours a yellow mixture was obtained which was concentrated under vacuum to remove the solvent and the residue was filtered, washed with diethylether and dried in air (Fig. 1).

Yield: 82% of yellow solid, m. p. 138°C. **UV–vis** (MeOH): $\lambda_{max(n)}$ (nm). $\lambda_{max(1)}$ (207), $\lambda_{max(2)}$ (237), $\lambda_{max(3)}$ (356.55). **IR** (Solid state), ν_x (cm^{-1}): $\nu_{C-H(aromatic)}$ (3086 3029), $\nu_{C-H(aliphatic)}$ (2941 2838), $\nu_{C=N}$ (1600), $\nu_{C=C(aromatic)}$ (1582 1522), $\nu_{C\ C=C(aromatic)}$ (1479), $\nu_{N(CH_3)_2}$ (1436 and 1359), $\nu_{C-N(aromatic)}$ (1230 1067), $\nu_{C-N(aliphatic)}$ (964), $\nu_{=C-H}$ (904), ν_{Ar-CH} (758). **^{1}H NMR** (300 MHz, $CDCl_3$), δ (ppm): 3.08 ppm (6H, s, C**H**$_3$–N–C**H**$_3$), 6.76–6.79 ppm (2H, d, J = 9.1 Hz, –C**H**$_{Ar}$–), 7.21 ppm (1H, s, –C**H**$_{Ar}$–),7.23–7.28 ppm (2H, m, –C**H**$_{Ar}$–), 7.40–7.44 ppm (2H, t, J = 7.7 Hz, –C**H**$_{Ar}$–), 7.82–7.85 ppm (2H, d, J = 8.9 Hz, –C**H**$_{Ar}$–), 8.38 ppm (1H, s, –C**H**=N-). **^{13}C NMR** (300 MHz, $CDCl_3$), δ (ppm): 40.06 ppm (2C, **C**H$_3$–N–**C**H$_3$), 111.63 ppm (2C, –**C**H$_{Ar}$–), 121.02 ppm (2C, –**C**H$_{Ar}$–), 124.51 and 125.03 ppm (2C, –**C**H$_{Ar}$), 129.09 ppm (2C, –**C**H$_{Ar}$), 130.5 ppm (2C, –**C**H$_{Ar}$), 152.56 (1C, –**C**H$_{Ar}$–), 153.05 (1C, –**C**H$_{Ar}$–), 160.29 (1C, –**C**H=N-).

2.2.2. Preparation of the α-aminophosphonate derivative

The studied α-aminophosphonate derivative, namely diethyl ((4-(dimethylamino) phenyl) (phenylamino) methyl) phosphonate (**α-APD**), was prepared by adding equimolar amount of diethylphosphite (1.0 mmol) to previous imine **E-NDPIMA** (1.0 mmol)

via pudovik reaction. The mixture was refluxed in toluene while stirring for an appropriate reaction time. After cooling, the formed liquid product solid was concentrated beneath lower pressure to obtain crude product, which were further cleaned and washed with diethylether several times and finally dried at room temperature (Fig. 1).

Yield: 78% of Yellowish orange solid, m. p. 112°C. **UV–vis** (MeOH): $\lambda_{max(n)}$ (nm): $\lambda_{max(1)}$ (205); $\lambda_{max(2)}$ (246), $\lambda_{max(3)}$ (265),; $\lambda_{max(4)}$ (301). **IR** (Solid state) ν_x (cm^{-1}): ν_{N-H} (3294), $\nu_{=C-H(aromatic)}$ (3037), $\nu_{C-H(aliphatic)}$ (2804–2985), $\nu_{C=C(aromatic)}$ (1601) and 1515), $\nu_{N(CH_3)_2}$ (1498), ν_{C-O} (1308), ν_{P-CH_2} (1360), ν_{P-O} (750), $\nu_{P=O}$ (1231,1162 and 1102), $\nu_{N-C(aliphatic)}$ (1017), $\nu_{C-C(aliphatic)}$ (939), ν_{C-P} (750 and 603), ν_{P-O-C} (690). **^{1}H NMR** (400 MHz, DMSO-d6), δ (ppm): 1.19 ppm (6H, t, J=6.9 Hz, $-CH_2-C\underline{H_3}$), 3.41 ppm (6H, s, $C\underline{H_3}-N-C\underline{H_3}$), 4.04 ppm (4H, m, $-C\underline{H_2}-CH_3$), 4.79 ppm (1H, d, J=9.7 Hz, $-C\underline{H}-N-$), 6.52 ppm (2H, t, J=6.4 Hz $-C\underline{H}_{Ar}-$), 6.75 ppm (2H, d, J=8.5 Hz, $-C\underline{H}_{Ar}-$), 7.01 ppm (2H, t, J=7.5 Hz $-C\underline{H}_{Ar}-$), 7.31 ppm (2H, m, $-C\underline{H}_{Ar}-$), 9.68 ppm (1H, s, $-N\underline{H}-C-$). **^{13}C NMR** (400 MHz, DMSO-d6), δ (ppm): 16.62 ppm (2C, $\underline{C}H_3-CH_2-$), 53.08 ppm (2C, $\underline{C}H_3-N-\underline{C}H_3$), 54.62 ppm (2C, $CH_3-\underline{C}H_2-$), 63.65 ppm (1C, $-\underline{C}H-N-$), 112.43 ppm (2C, $-\underline{C}H_{Ar}-$), 114.06 ppm (2C, $-\underline{C}H_{Ar}-$), 117.19 ppm (1C, $-\underline{C}H_{Ar}-$), 124.15 ppm (1C, $-\underline{C}H_{Ar}-$), 129.06 ppm (2C, $-\underline{C}H_{Ar}-$), 129.42 ppm (2C, $-\underline{C}H_{Ar}$), 147.86 ppm (1C, $-\underline{C}H_{Ar}-$), 150.23 (1C, $-\underline{C}H_{Ar}-$).**^{31}P NMR** (400 MHz, DMSO-d6), δ (ppm): 23.562 ppm (C-$\underline{P}O(OC_2H_5)_2$).

From the results of section 2.2.1 and 2.2.2 we can note that:

- ➢ - The UV–Vis spectra shown that the synthetic products are characterized by wavelengths (λ_{max}) quite different from those of the utilized starting reagents.
- ➢ The ATR-FTR showed clearly the disappearance of the characteristic peaks of the $-NH_2$ function of aniline and the carbonyl group C=O of 4-(dimethylamino)benzaldehyde, and the appearance of the attributed peak of the formation of C=N function on the Schiff base spectrum, and the formation of P=O, C–N and N–H functions on the α-aminophosphonic derivative spectrum.
- ➢ The chemical shifts, the coupling constants and the presence of a single peak of phosphorus on the ^{31}P NMR spectrum of the α-APD compound.
- ➢ The melting points of the concerned compounds are very different.

All of these results confirm the obtaining of the new products and the proposed structures.

2.3. Gravimetric proceedings

All the gravimetric essays were implemented at temperature constant (25 °C) in all tests. The immersion time of steel specimens in 0.5 mol L^{-1} H_2SO_4 solutions with and without of inhibitors was around 24 h. The carbon steel specimens were isolated from the examined solutions, cleaned carefully with distilled water succeed by acetone and desiccated with warm air using an electric dryer, then weighed for a second time. Gravimetric study was applied to determine the corrosion rate (A_{corr}), the surface coverage (θ) and inhibition efficiency ($\eta_{W\square}$(%)) as follows:

$$A_{corr} = \frac{\Delta W}{S \times t} = \frac{W_1 - W_2}{S \times t} \quad (1)$$

$$\theta = \frac{A^0_{corr} - A_{corr}}{A^0_{corr}} \quad (2)$$

$$\eta_W(\%) = \frac{A^0_{corr} - A_{corr}}{A^0_{corr}} \times 100 \quad (3)$$

where W_1 and W_2 are the sample mass before and after plunge in the examined solution respectively, S is the surface area of the sample and t is the finish time of every experience, A^0_{corr} is a corrosion rate in absence of the inhibitor and A_{corr} is a corrosion rate in presence of the inhibitor.

2.4. Electrochemical proceedings

Electrochemical measurements were accomplished in an usual three electrode compartment with carbon as auxiliary electrode (CE), a calomel electrode (SCE) as the reference electrode (RE) and a XC48 carbon steel as the working electrode (WE). Firstly, the working electrode was introduced in the studied solution at 25 °C and after founding a stable state, the electrochemical measurements were realized in a Dell 8284 machine monitored electrochemical workstation (PGZ 310 Voltalab40). The experimental results were traced and evaluated employing Voltamaster 4 software. The potentiodynamic polarization curves were obtained in potential domain from −800 to −200 (mV/SCE) with a scan rate of 0.5 mV s^{-1}. The following equation is applied to determine the inhibition efficiency established from the polarization data (η_p (%)) [31]:

$$\eta_p(\%) = \left(\frac{i_{corr(inh)} - i^{\circ}_{corr}}{i_{corr(inh)}}\right) \times 100 \quad (4)$$

where i°_{corr} and $i_{corr(inh)}$ are the corrosion current density values in the absence and presence of inhibitor respectively.

Electrochemical impedance spectroscopy (EIS) measurements were realized with amplitude signal perturbation of 5 mV AC sine wave with the frequency domain from 100 kHz to 10 mHz. The inhibition effectiveness determinated from EIS measurements (η_z(%)) was obtained employing the following formula [31]:

$$\eta_z(\%) = \left(\frac{R'_P - R_P}{R'_P}\right) \times 100 \quad (5)$$

where R'_P and R_P are the charge transfer resistance values with and without the presence of the investigated inhibitors, respectively.

2.5. Surface analysis

The carbon steel specimen surfaces exposed to 0.5 mol L^{-1} H_2SO_4 solution in absence and in presence of 10^{-3} mol L^{-1} of the investigated inhibitors were examined by Atomic Force Microscopy (AFM) for an immersion duration of 24 h at 25 °C, by employing an Asylum Research MFP-3D Classic AFM appliance.

2.6. Quantum chemical calculations

All quantum chemical calculations were executed with total geometry optimizations applying usual Gaussian 09 W program parcel [32] and the obtained results were visualized by means of GaussView 5.0.8 computer software [33]. Geometry optimization was carried out by Density Functional Theory (DFT) with the Beck's

three parameter exchange functional and the Lee–Yang–Parr non-local correlation functional (B3LYP) with 6–31G (d, p) basis set [34].

The values of E_{HOMO} and E_{LUMO} have been used to calculate all the quantum chemical parameters such as energy gap ΔE_{GAP} (E_{HOMO} E_{LUMO}), global hardness (η), global softness (σ), absolute electronegativity (χ), electrophilicity index (ω) and fraction of transferred electrons (ΔN). Also, the following equations were employed to determine the all precedent parameters [35–37]:

$$\eta = \frac{E_{LUMO} - E_{HOMO}}{2} \quad (6)$$

$$\sigma = \frac{1}{\eta} \quad (7)$$

$$\chi = \frac{-(E_{HOMO} + E_{LUMO})}{2} \quad (8)$$

$$\omega = \frac{\chi^2}{2\eta} \quad (9)$$

$$\Delta N = \frac{\chi_{Fe} - \chi_{inh}}{[2(\eta_{Fe} + \eta_{inh})]} \quad (10)$$

where:

χ_{Fe} and χ_{inh} are the absolute electronegativity of metal and inhibitor molecules respectively.

η_{Fe} and η_{inh} are the absolute hardness of metal and the inhibitor molecules, respectively.

For the calculation of fraction of transferred electrons we apply the theoretical values of $\chi_{Fe} = 7.0$ eV and $\eta_{Fe} = 0$ [38].

2.7. Molecular dynamics simulations

The Materials Studio 7.0 software was used to perform the molecular dynamics simulations (MDS) [39]. In this study we select the Fe (100) surface for the simulations of adsorption modes of the studied compounds on the Fe interface. The simulation box used for realized the MD simulations, has the dimensions of (17.20 Å × 22.93 Å × 22.93 Å) with periodic boundary conditions. The iron slab, the water slab comprising the investigated compounds and a vacuum film are involved in the simulation box. The Fe (100) surface and the molecular geometries of the studied inhibitors in gas and aqueous states were first optimized to minimum energy. The MD simulations were performed at 298 K, NVT ensemble, with a time step of 0.1 fs and simulation period of 50 ps using the COMPASS force field. The following equation was used to determine the interaction energy ($E_{interaction}$) between the inhibitors molecules and the Fe (100) interface:

$$E_{interaction} = E_{total} - E_{Fe+H_2O} - E_{inh} \quad (11)$$

where E_{total} is the total energy of the simulation system, E_{Fe+H_2O} is the energy of Fe surface simultaneously with water molecules, and E_{inh} is the energy of the alone inhibitor molecule. The binding energy ($E_{binding}$) is the negative value of $E_{interaction}$:

$$E_{binding} = -E_{interaction} \quad (12)$$

3. Results and discussions

3.1. Weight loss measurements

Weight loss measurements for carbon steel after 24 h of insertion in 0.5 mol L^{-1} H_2SO_4 solutions in the nonexistence and existence of different concentrations of inhibitors are regrouped in Table 1. Fig. 2 clearly shows that the inhibition effectiveness rises with rising inhibitors concentrations while corrosion rate reduces with increasing inhibitors concentrations. The weight loss results in Table 1, indicate that the highest value of $\eta_{W\square}$(%) was observed at 10^{-3} mol L^{-1} of inhibitors. There is an augmentation in the surface region protected by the adsorbed molecules on the iron surface with the rise in the inhibitors concentration. The effectiveness of the studied inhibitors is consequent to the existence of N, O and P contributors as well as the existence of π-electrons in aromatic rings. The corrosion rate and the inhibition effectiveness of the studied compounds pursue the sequence: A_{corr} α-APD < A_{corr} E-NDPIMA and $\eta_{W\square}$α-APD > $\eta_{W\square}$E-NDPIMA respectively. The highest inhibition effectiveness of the α-aminophosphonate derivative may be attributed to the existence of the phosphonate groups ($PO(OC_2H_5)_2$).

3.2. Tafel polarization measurements

The polarization graphs for carbon steel immersed in 0.5 mol L^{-1} H_2SO_4 at 25 °C in absence and in presence of different concentrations of the considered inhibitors are revealed in Fig. 3. The principal parameters extracted from polarization curves such as corrosion potential (E_{corr}), corrosion current density (i_{corr}), anodic and cathodic Tafel slopes (β_a and β_c), surface recovery rate (θ) and inhibitor effectiveness (η_p (%)) are presented in Table 2. We can see from the findings given in Fig. 3 and Table 2 that increasing inhibitors concentration decreased i_{corr} and increased η_p(%) significantly at all studied concentrations. Fig. 3 demonstrates that

Table 1
Corrosion rate and inhibition effectiveness data determined from weight loss measurements for XC48 carbon steel in 0.5 mol L^{-1} H_2SO_4 solutions in absence and presence of various concentrations of the **α-APD** and **E-NDPIMA** molecules at 25 °C.

Inhibitor	C (mol L^{-1})	W_i (g)	W_{24h} (g)	ΔW (g)	A_{corr} (g/cm^2h)	θ	η_w (%)
α-APD	Blank	13.40271	13.34027	0.062440	0.0002761854	–	–
	10^{-5}	12.97476	12.95808	0.016680	0.0000753796	0.7271	72.71
	5×10^{-5}	12.85015	12.83662	0.013530	0.0000639172	0.7686	76.86
	10^{-4}	12.97308	12.96148	0.011600	0.0000546757	0.8020	80.20
	5×10^{-4}	13.28260	13.27626	0.006340	0.0000280432	0.8985	89.85
	10^{-3}	12.42394	12.41982	0.004120	0.0000198459	0.9281	92.81
E-NDPIMA	Blank	13.25221	13.18800	0.064210	0.0002840145	–	–
	10^{-5}	13.34086	13.32075	0.020110	0.0000908803	0.6800	68.00
	5×10^{-5}	13.01846	13.00139	0.017070	0.0000789401	0.7221	72.21
	10^{-4}	12.98122	12.96651	0.014710	0.0000686357	0.7583	75.83
	5×10^{-4}	13.20884	13.19549	0.013350	0.0000590499	0.7921	79.21
	10^{-3}	13.21232	13.20322	0.009100	0.0000402512	0.8583	85.83

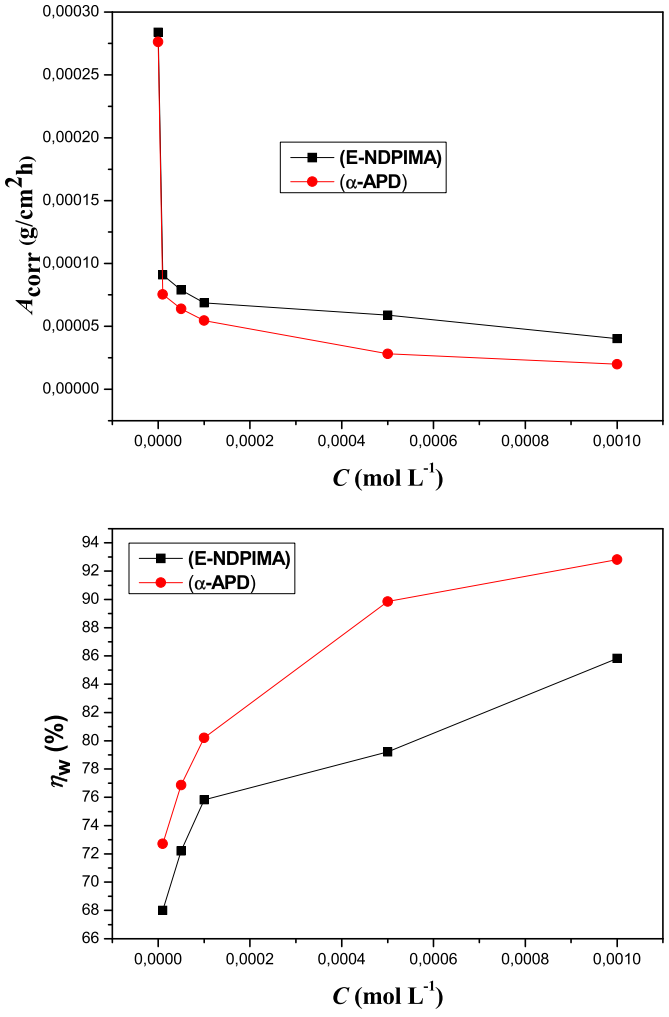

Fig. 2. Relation between corrosion rate A_{corr}, inhibition efficiency η_w(%) and concentration of inhibitors **E-NDPIMA** and **α-APD** in 0.5 mol L^{-1} H_2SO_4 established by weight loss method at 25 °C.

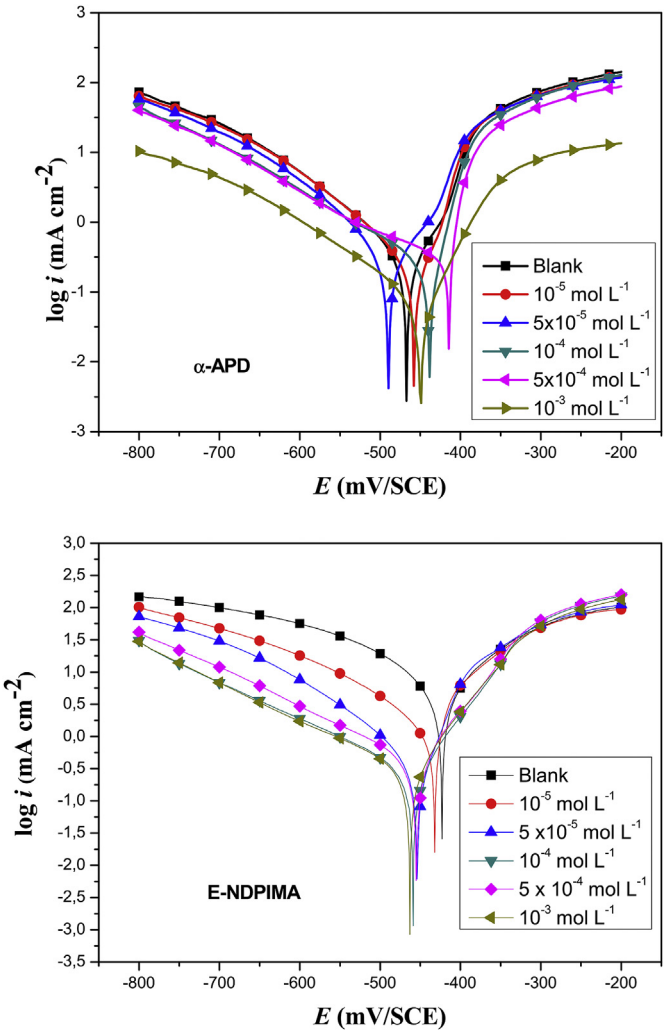

Fig. 3. Polarization diagrams of carbon steel in 0.5 mol L^{-1} H_2SO_4 including various concentrations of inhibitors at 25 °C: **α-APD:** diethyl ((4-(dimethylamino)phenyl)(-phenylamino)methyl)phosphonate **E-NDPIMA:** (E)-N,N-dimethyl-4-((phenylimino) methyl)aniline.

in existence of the studied inhibitors the cathodic and anodic sections of the polarization diagrams are displaced in the direction of lower currents to equal extent, this perhaps due to the obstructing impact of the adsorbed inhibitors molecules. Moreover, this result indicates that the considered derivatives inhibit corrosion by monitoring together anodic and cathodic reactions (mixed type inhibitors). As well, the presence of the **α-APD** and **E-NDPIMA** inhibitors decreases the anodic dissolution of iron and also delays the cathodic reactions of hydrogen progression [40,41]. In the current research the maximum values of the inhibition efficiency ware 93% for **α-APD** and 86% for **E-NDPIMA** at 10^{-3} mol L^{-1}, indicating that the studied inhibitors protects the surface of the carbon steel by forming of an adsorptive layer of its molecules.

3.3. Electrochemical impedance measurements

Fig. 4 presents the Nyquist diagrams of carbon steel in 0.5 mol L^{-1} H_2SO_4 in nonexistence and existence of various concentrations of the studied inhibitors at 25 °C. According to Nyquist diagrams we observe one capacitive buckle was obtained either in the nonexistence or existence of inhibitors. This indicates that oxidation of carbon steel in 0.5 mol L^{-1} H_2SO_4 solution is mostly restricted by the charge movement procedure [42,43]. Furthermore, the obtained Nyquist graphs for all the examined concentrations are nearly semi-circles and demonstrate identical forms. This shows that no significant modification in the corrosion mechanism arises as a consequence of the inhibitors adding [44]. In effect such phenomenon as usually attributed to the frequency dispersal which is assigned to the surface heterogeneity generating from the roughness of the surface and chemical content of carbon steel [45]. Moreover, the diameters of the capacitive buckles rise with rising inhibitors concentration, which may be associated to the augmentation of surface coverage of inhibitive compounds on carbon steel surface [46]. In addition, an equivalent circuit was utilized to examine the EIS diagrams of all tests and to model the iron/solution interface, the results are summarized in Table 3 [47], which is contain the solution resistance (R_s), the resistance of charge transfer (R_{ct}) and the capacitance of charge transfer (C_{dl}).

3.4. Adsorption isotherm

Generally the organic molecules protect the metals surface against corrosion by adsorption. Essential information concerning the interactions between the inhibitors molecules and the metal surface may be offered by the adsorption isotherm. Several

Table 2
Potentiodynamic polarization parameters for the corrosion of carbon steel in 0.5 mol L^{-1} H_2SO_4 solution including various concentrations of the **α-APD** and **E-NDPIMA** inhibitors at 25 °C.

Inhibitor	C_{Inh}(mol L^{-1})	E_{corr} (mV/SCE)	i_{corr} (mA/cm^2)	β_a (mV/dec.)	β_c (mV/dec.)	η_p(%)	θ
α-APD	Blank	− 489.5	1.2582	257.9	− 288.4	–	–
	10^{-5}	− 466.8	0.3488	50.6	− 111.7	72.28	0.7228
	5×10^{-5}	− 457.6	0.2889	39.8	− 111.9	77.04	0.7704
	10^{-4}	− 438.2	0.2074	28.4	− 140.6	83.52	0.8352
	5×10^{-4}	− 414.6	0.1384	19.6	− 139.0	89.00	0.8900
	10^{-3}	− 448.2	0.0940	59.1	− 142.1	92.53	0.9253
E-NDPIMA	Blank	− 422.9	1.4829	37.6	− 45.60	–	–
	10^{-5}	− 432.3	0.4882	22.3	− 49.80	67.08	0.6708
	5×10^{-5}	− 453.7	0.4345	45.9	− 112.2	70.70	0.7070
	10^{-4}	− 458.8	0.3440	66.3	− 190.8	76.80	0.7680
	5×10^{-4}	− 454.8	0.2968	57.2	− 112.8	79.98	0.7998
	10^{-3}	− 463.0	0.2034	57.7	− 108.8	86.26	0.8626

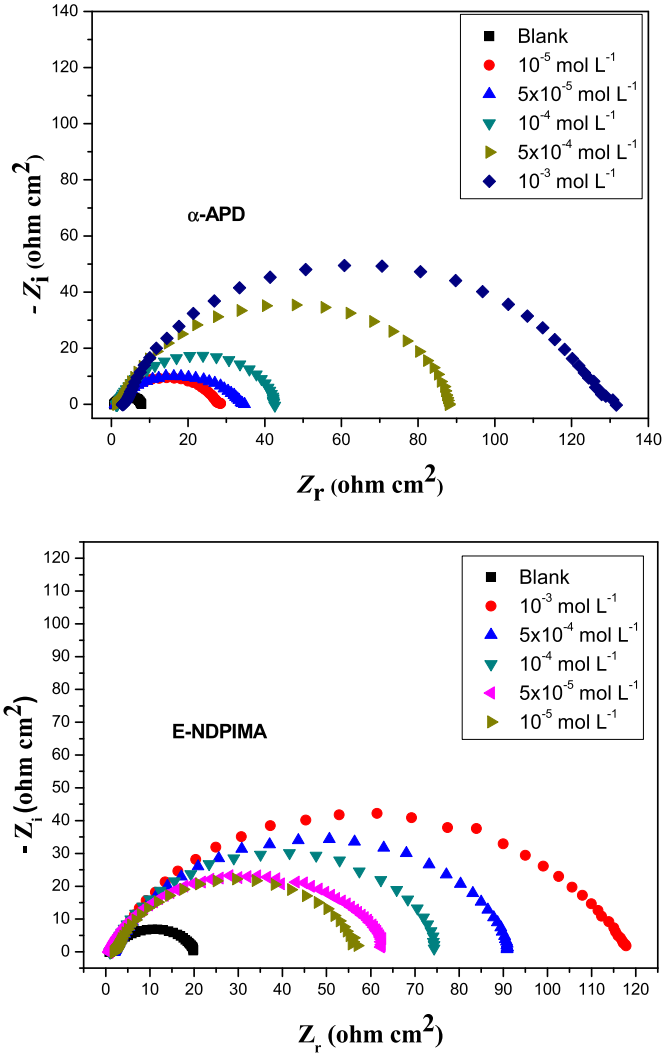

Fig. 4. Nyquist diagrams of the corrosion of carbon steel in 0.5 mol L^{-1} H_2SO_4 without and with various concentrations of inhibitors at 25 °C: **α-APD**: diethyl ((4-(dimethylamino) phenyl) (phenylamino) methyl) phosphonate, **E-NDPIMA**: (E)-N, N-dimethyl-4-((phenylimino) methyl) aniline.

adsorption isotherms are widely employed to fit the surface coverage (θ) values at different concentrations of the inhibitor, among them those of Frumkin, Langmuir, Temkin and Freundlich [48]. Modeling the adsorption isotherm of corrosion results is an important pathway for foretelling the adsorption behavior.

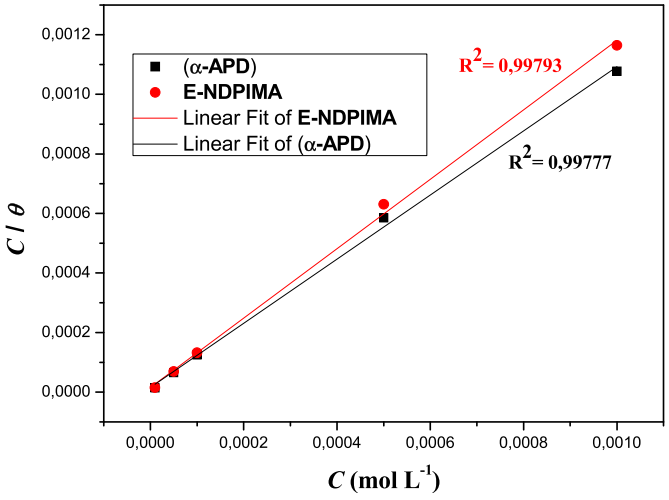

Fig. 5. Langmuir isotherm adsorption plot of the **α-APD** and **E-NDPIMA** on the iron surface in 0.5 mol L^{-1} H_2SO_4 at 25 °C established from weight loss measurement.

Furthermore, the linear regression of isotherm results into isotherm models is an alternate mathematical method widely employed to foresee the global adsorption conductance. The linear form of the Langmuir isotherm model is known by the following equation [49]:

$$\frac{C}{\theta} = \frac{1}{K_{ads}} + C \tag{13}$$

where C_{inh} is the inhibitor concentration (mol L^{-1}) and K_{ads} is the adsorption equilibrium constant ((mol L^{-1})$^{-1}$). It can be observed from Fig. 5 that the graph of the linear fit of C_{inh}/θ versus C_{inh} for both studied inhibitors are a right lines with a medium correlation coefficients nearly equals to 1 ($R^2 = 0.99843$ and $R^2 = 0.9977$), these suggest that the adsorption of the studied inhibitors molecules on the iron surface follow Langmuir isotherm. As shown, the values of K_{ads} determined using Langmuir model was 65153.79 (mol L^{-1})$^{-1}$ and 64004.51 (mol L^{-1})$^{-1}$ for **α-APD** and **E-NDPIMA** respectively. Also, we observe that the studied inhibitors present high values of the adsorption equilibrium constants, these suggest a powerful interaction between the studied molecules and the iron surface [50]. As well K_{ads} of **α-APD** is highest than K_{ads} of **E-NDPIMA,** this probably referred to the presence of the phosphonic group (O═P(OC_2H_5)$_2$) in the **α-APD** molecular structure. The obtained values of K_{ads} can be used to calculate the standard Gibbs free energy of adsorption ($-\Delta G^0_{ads}$) using the following equation [47]:

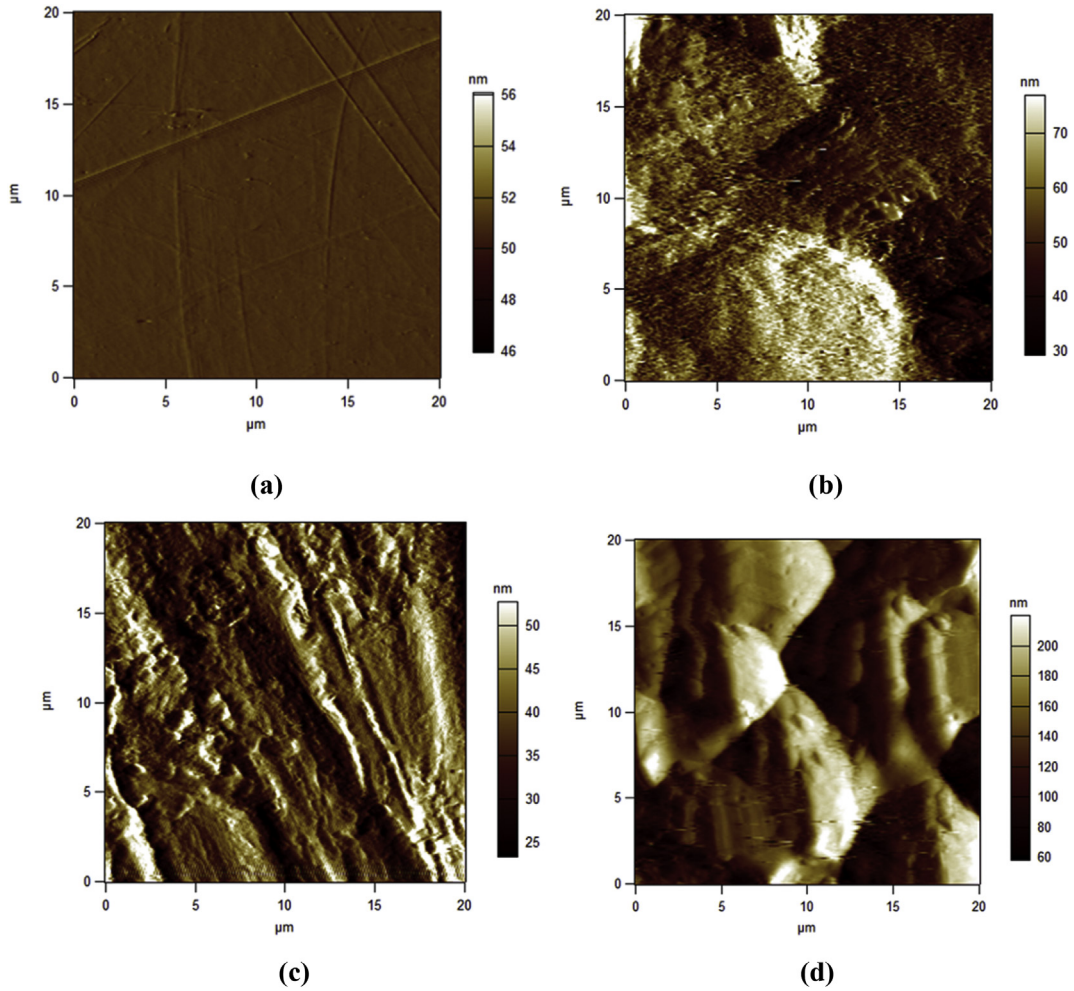

Fig. 6. AFM images of the carbon steel surface: (**a**) before immersion (**b**) after 24 h immersion in 0.5 mol L^{-1} H_2SO_4 (**c**) after 24 h immersion in 0.5 mol L^{-1} H_2SO_4 in presence of 10^{-3} mol L^{-1} of **α-APD** (**d**) after 24 h immersion in 0.5 mol L^{-1} H_2SO_4 in presence of10^{-3} mol L^{-1} of **E-NDPIMA.**

Table 3
Electrochemical parameters obtained from EIS measurements on XC48 carbon steel in 0.5 mol L^{-1} H_2SO_4 solutions without and with different concentrations of the **α-APD** and **E-NDPIMA** inhibitors at 25 °C using corresponding equivalent circuit.

Inhibitor	C_{Inh} (mol L^{-1})	R_2 (Ω cm^2)	C_{dl} (µF cm^{-2})	R_1 (Ω cm^2)	η_z (%)
α-APD	Blank	07.032	1131	0.893	–
	10^{-5}	26.33	604.3	1.455	73.08
	5×10^{-5}	32.99	304.8	1.154	78.41
	10^{-4}	40.73	976.7	1.787	82.74
	5×10^{-4}	86.68	580.1	2.021	91.89
	10^{-3}	122.7	515.6	3.424	94.27
E-NDPIMA	Blank	19.03	1053	1.185	–
	10^{-5}	54.83	725.5	2.154	64.81
	5×10^{-5}	62.89	354.2	887.2	69.35
	10^{-4}	73.96	271.1	1.494	74.27
	5×10^{-4}	89.62	177.5	2.202	78.76
	10^{-3}	116.4	172.2	1.315	83.65

$$\Delta G^0_{ads} = -RT \ln(55.5K_{ads}) \quad (14)$$

where R is the gas constant (8.314 J K^{-1} mol^{-1}), T the absolute temperature (K), the value 55.5 is the concentration of water in the solution given in mol L^{-1}. The obtained values of $-\Delta G^0_{ads}$ for **α-APD** and **E-NDPIMA** are −36.786 kJ mol^{-1} and −36.742 kJ mol^{-1} respectively. The negative values of $-\Delta G^0_{ads}$ ensure the spontaneous adsorption process on the iron surface [51].

Generally, there are two kinds of interactions can explain the adsorption of organic molecules on the metal surface: physical and chemical interactions. In principle, values of $-\Delta G^0_{ads}$ about to 20 kJ mol^{-1} are proportionate with electrostatic interactions between the charged molecules and charged metal (physical adsorption), The ΔG values near 40 kJ mol^{-1} or higher indicate that are related with chemisorption either with the participation or transfer of electrons from organic molecules to the metal surface to shape a coordinate type of bond (chemical adsorption) [52,53]. For the studied inhibitors, the obtained values of $-\Delta G^0_{ads}$ are ranging from −40 to −20 kJ mol^{-1}. Therefore, **α-APD** and **E-NDPIMA** molecules adsorbed on the iron surface mostly by an association of a chemical and a physical adsorption.

3.5. Atomic force microscopy observations

AFM analyses were conducted in order to study the surface morphology and it is very advantageous to characterize the protective layer formed on the carbon steel surface. AFM images of iron surface before and after 24 h of insertion in 0.5 mol L^{-1} H_2SO_4 solution without and with the existence of the studied inhibitors are exposed in Fig. 6. The calculated medium roughness of furbished

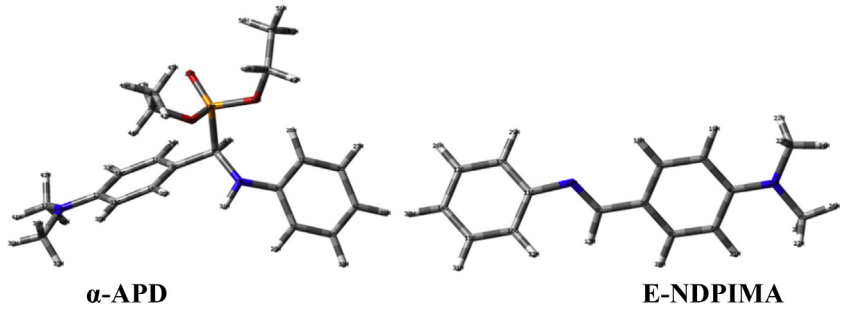

(a) Optimized molecular structures.

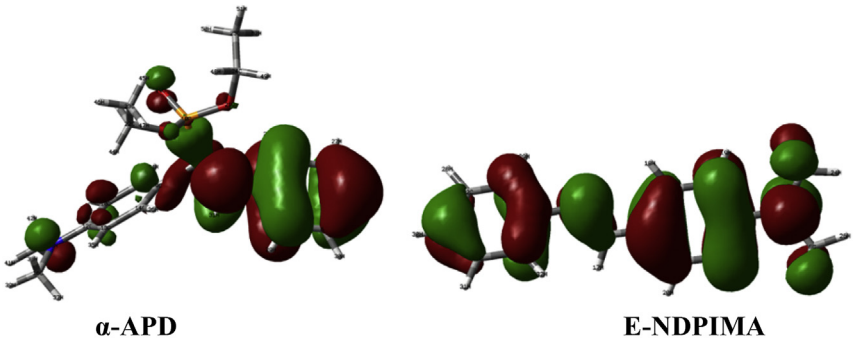

(b) HOMO.

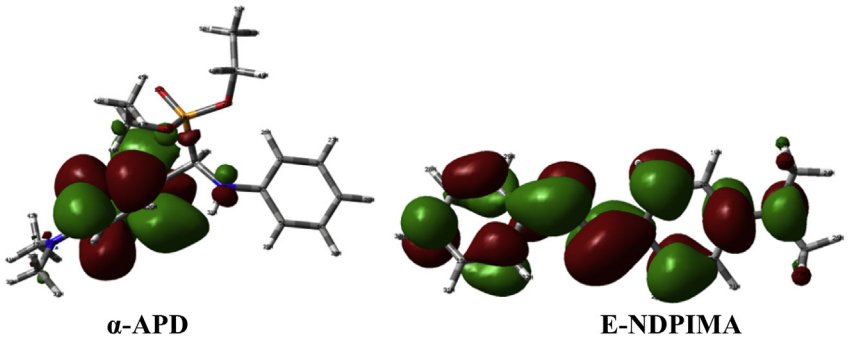

(c) LUMO.

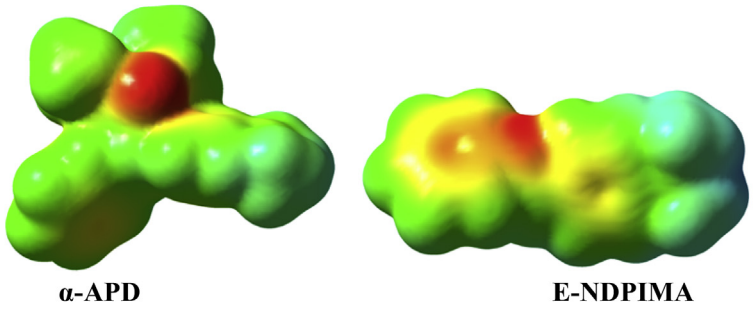

(d) MEP

Fig. 7. Optimized molecular structures, molecular orbitals density distributions and the MEP maps of the **α-APD** and **E-NDPIMA**.

carbon steel prior and next insertion in 0.5 mol L^{-1} H_2SO_4 solution in nonexistence of corrosion inhibitors was calculated as 51.004 and 405.320 nm, respectively (Fig. 6(a) and 6(b)). The high value of average roughness obtained after immersion in nonexistence of the investigated inhibitors is owing to aggressive attack by acid solution. However, in the existence of 10^{-3} mol L^{-1} of **α-APD** and **E-NDPIMA,** the calculated average roughness of carbon steel surface was diminished to 176.436 nm and 275.805 nm respectively (Fig. 6(c) and 6(d)); this confirms the formation of protective surface layer by inhibitors, which performed in diminished corrosion rate and surface deterioration of iron.

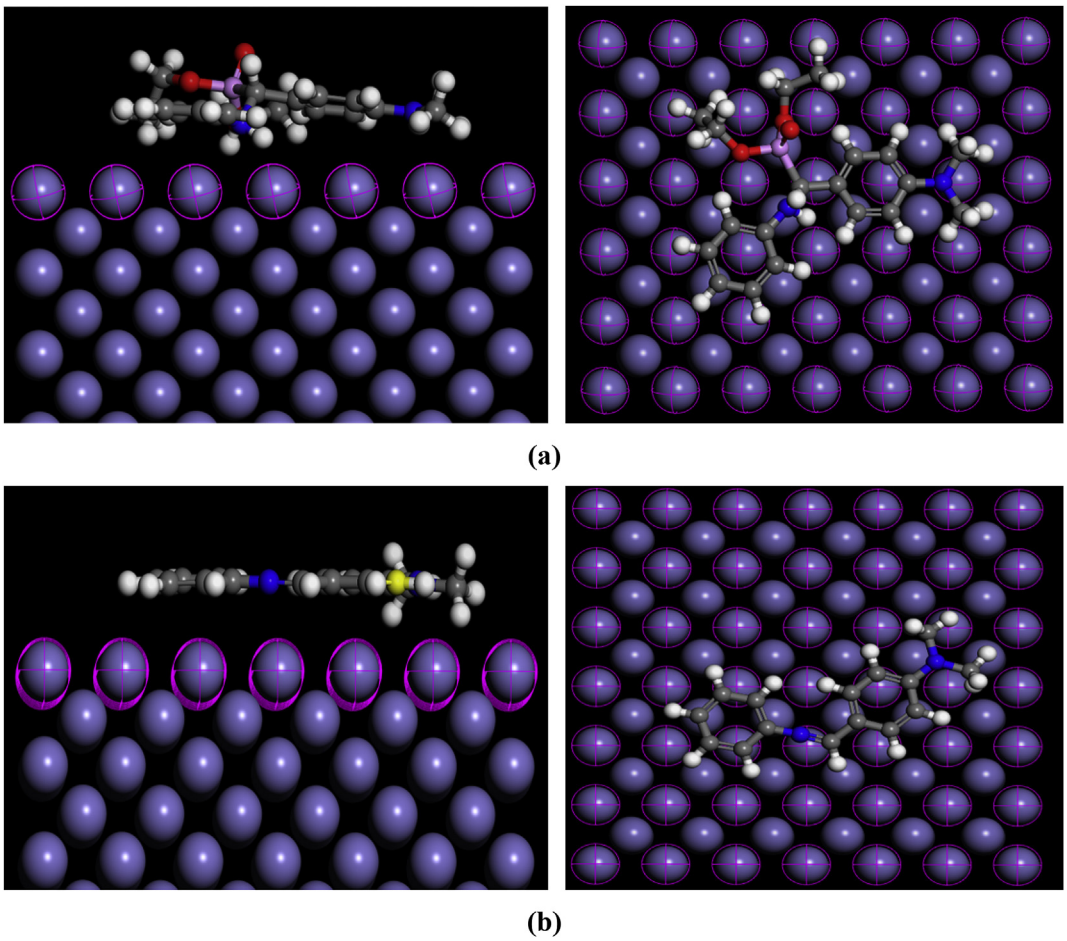

Fig. 8. Final configurations of the adsorbed molecules on Fe (100) surface vacuum slab: **(a) α-APD (b) E-NDPIMA**.

3.6. Quantum chemical computations

In order to investigate the relationship between the molecular structures of the **α-APD** and **E-NDPIMA** and the inhibition efficiency of these compounds, several quantum chemical computations were carried out. Quantum chemical factors such as the energies of highest occupied molecular orbital (E_{HOMO}) and the lowest unoccupied molecular orbital (E_{LUMO}), the energy variation (ΔE_{gap}) between E_{HOMO} and E_{LUMO}, electronegativity (χ), electron affinity (A), dipole moment (μ), global hardness (η), softness (σ), ionization potential (I), the global electrophilicity (ω), the portion of electrons transported (ΔN), the total energy (E_T) and Mullikan charges on the backbone atoms have been obtained from DFT calculations using B3LYP level with basis set 6-31G(d,p) method. All quantum chemical parameters were achieved afterward geometric optimization and the obtained results are given in Table 4. The optimized structures, HOMO and LUMO orbitals of the **α-APD** and **E-NDPIMA** molecules are presented in Fig. 7 (a), 7(b) and 7(c). Generally, the HOMO is related to the electron contributing capacity of an inhibitor. The elevated values of E_{HOMO} are indicating also, the ability of the inhibitor to give electrons to suitable receptor molecules. The spatial distribution of electrons is determined by the HOMO orbital, electrophilic attacks can be correlated very well with atomic sites having high density of the HOMO orbital. As may be seen from Fig. 7(b) and 7(c)Figs. 7(b) and 7(c), that the HOMO is found to reside on the benzene ring and heteroatoms for the tow studied derivatives. On the other hand, the LUMO is associated to the capability of the inhibitor to take electrons. As well, the low value of E_{LUMO} indicates that the electron accepting capability of the inhibitor is higher. Furthermore, the energy difference between LUMO and HOMO (ΔE_{gap}) is a factor with the minimum value causes elevated inhibition efficiency of the inhibitor [54,55]. Generally, the created complex on the metal surface is highly steady when the value of ΔE_{GAP} is low, which improves the inhibition efficiency of the inhibitor [56]. It can be seen from Table 4 that ΔE_{GAP} of **α-APD** is less than that of **E-NDPIMA,** this indicates that **α-APD** derivative could have preferable performances as corrosion inhibitor than **E-NDPIMA** molecule, a conclusion which is in total accord with the experimental findings.

Table 4
Obtained quantum chemical parameters of the **α-APD** and **E-NDPIMA** inhibitors.

Quantum chemical parameter	α-APD	E-NDPIMA
E_{Tot} (eV)	− 38555.83266	− 18796.16611
E_{HOMO} (eV)	− 5.060776172	− 5.08445009
E_{LUMO} (eV)	− 0.105308118	− 0.096075192
ΔE_{GAP} (eV)	− 4.955468054	− 4.988374898
μ (Debye)	4.52310	4.05647
η (eV)	2.4777342496	2.494187449
σ	0.40359453406	0.400932175487024
χ (eV)	2.583042145	2.590262641
ω	1.34641290201387	1.34501930719969
ΔN	0.891330023732986	0.884002796335136

The dipole moment (μ) is an additional quantum chemical factor used to discuss the corrosion inhibition efficiency of a molecule. Several researchers have shown that the dipole moment is

resultant to the polarity of an inhibitor and the elevated values of μ are answerable for great inhibition effectiveness [57,58]. Table 4 shows that the dipole moment of **α-APD** is greater than that of **E-NDPIMA** molecule, which shows the high efficiency of **α-APD**, this probably due to the existence of the phosphonate group in its molecular structure. In general, the capability of the inhibitor molecules to take electrons is illustrated by the electrophilicity index (ω). Furthermore, the decrease of the ω value increases the inhibition efficiency. Table 4 elucidates that the values of ω of the examined inhibitors follow the order of **E-NDPIMA** > **α-APD**, which shows higher efficiency of **α-APD**.

The number of electrons transferred (ΔN) is a significant factor to evaluate the corrosion inhibition efficiency of organic compounds. So, the ΔN values of the studied inhibitors were obtained and regrouped in Table 4. Values of ΔN demonstrate that the inhibition effectiveness producing from electron contribution accord with Lukovits's research [59]. It known in literature that for the values of $\Delta N < 3.6$, the inhibition effectiveness raises the electrons donating capability at the metal surface [59]. As seen from Table 4, the ΔN of **α-APD** is highest of the **E-NDPIMA**, this result shows that ΔN values correlates powerfully with the obtained experimental efficiencies. Consequently, the great ΔN is related with the excellent inhibitor (**α-APD**), while the smallest amount is related with the compound that has the low inhibition effectiveness (**E-NDPIMA**).

The Mulliken charges of the studied inhibitors were given in Table 5. Generally, the Mulliken charge of atoms in inhibitors molecules is defined the adsorption center. In Table 5, the more negative charges of the **α-APD** and **E-NDPIMA** molecules ware located on N7, O19, O20, O21, and N15 atoms and N33 and N10 atoms, respectively. This suggests that these atoms are probably the active adsorptive sites.

The use of the molecular electrostatic potential maps (MEP) is a helpful indicator to determine the efficient centers accountable for electrophilic and nucleophilic reactions. Moreover, MEP is associated to the electronic density. To determine reactive centers for electrophilic and nucleophilic attack, MEP maps of the investigated inhibitors are calculated at the optimized geometries. The visualization of the Fig. 7(d) shows that red and yellow tints illustrate the negative zones of the MEP associated to electrophilic reactivity, while the blue tint represents the positive zones related to nucleophilic reactivity. Obviously through Fig. 7(d) that for the considered inhibitors, the possible sites for electrophilic attack are generally located at heteroatom. Otherwise, the phenyl rings of the considered compounds have a negative region. It is clear from the obtained zones of MEP that the negative possible positions are about electronegative atoms (N and O) and the conjugated double bonds, contrariwise the positive possible zones are about the hydrogen atoms.

Table 5
Obtained Mullikan atomic charges of the **α-APD** and **E-NDPIMA** inhibitors.

α-APD		E-NDPIMA	
Atom	Mulliken Charge	Atom	Mulliken Charge
C1	− 0.1068270	C1	− 0.1181080
C2	− 0.1014860	C2	− 0.1324390
C3	0.3124670	C3	0.0909010
C4	− 0.0942550	C4	0.3548210
C5	− 0.1334350	C5	− 0.1406310
C6	− 0.0897730	C6	− 0.1388880
N7	− 0.5853780	C7	− 0.1691790
C8	− 0.1767240	C8	− 0.1686960
C9	0.0651930	C9	0.1051150
C10	− 0.1322960	N10	− 0.4935910
C11	− 0.1146190	C11	0.2444080
C12	0.3509800	C12	− 0.0933880
C13	− 0.1381020	C13	− 0.0944140
C14	− 0.1408830	C14	− 0.0857030
N15	− 0.5073060	C15	− 0.0984680
C16	− 0.1677690	C16	− 0.0986480
C17	− 0.1689680	N33	− 0.5076200
P18	1.1774370	–	–
O19	− 0.5772980	–	–
O20	− 0.5627780	–	–
O21	− 0.5407280	–	–
C22	0.0429750	–	–
C23	− 0.3281780	–	–
C24	0.0453330	–	–
C25	− 0.3335600	–	–

3.7. Molecular dynamic simulations

The study of the adsorption behavior of the **α-APD** and **E-NDPIMA** inhibitors on the Fe (100) surface was performed utilizing molecular dynamic simulations (MDS). Thus, the obtained equilibrium configurations of **α-APD** and **E-NDPIMA** inhibitors on the Fe (100) surfaces in a vacuum slab are shown in Fig. 8. It can be seen from Fig. 8 that the investigated inhibitors are adsorbed on the Fe (100) surface with nearly a horizontal manner. These adsorption configurations indicate the sturdy interactions between the studied inhibitors molecules and steel atoms. Inspection of the molecular structures of the studied inhibitors demonstrates that the adsorption on metal surface is take place by the involvement of the electrons of nitrogen, oxygen and the aromatic rings of the inhibitors molecules with those of iron, which leads to the creation of coordinate bonds (chemical interactions) [13]. Additionally, the Van der Waals dispersion forces are discussing the physical interactions between the inhibitors molecules and the metal surface [60]. Table 6 summarizes the calculated values of the interaction energy and binding energy of the examined compounds. As can be seen from Table 6, the negative values of the interaction energy indicate the spontaneity of the adsorption procedure. In principle, the high value of binding energy is related to most rigid molecules/surface interactions [61]. We can see from Table 6 that **α-APD** molecules have a high binding energy indicates **α-APD** can easily adsorb on the Fe (100) surface and exhibits high inhibition efficiency.

4. Conclusions

Our study has drowned several remarkable conclusions. Firstly, tow new α-aminophosphonate and Schiff base derivatives have been prepared and characterized by the spectroscopic techniques. Both studied compounds reveal high inhibition activities towards the corrosion of XC48 carbon steel in a 0.5 mol L^{-1} H_2SO_4 medium. The inhibition effectiveness increment with the increasing concentration of the two inhibitors and the α-aminophosphonate derivative presents the best inhibition effectiveness. The potentiodynamic polarization measurements show that **α-APD** and **E-NDPIMA** act as mixed type inhibitors. Moreover, EIS measurements illustrate that the presence of the **α-APD** and **E-NDPIMA** molecules increases the R_{ct} values while lowering C_{dl} values. In addition, the adsorption process of **α-APD** and **E-NDPIMA** molecules on iron surface follows the Langmuir adsorption isotherm. As well, the obtained negative values of the ΔG^0_{ads} elucidate the spontaneous process adsorption and the great interactions of the **α-**

Table 6
Calculated interaction and binding energies between the **α-APD** and **E-NDPIMA** inhibitors and Fe (100) surface.

Systems	$E_{Interaction}$ (kJ mol^{-1})	$E_{binding}$ (kJ mol^{-1})
Fe + **α-APD**	− 510.850220577	510.850220577
Fe + **E-NDPIMA**	− 124.16468681	124.16468681

APD and **E-NDPIMA** molecules with the metal surface. Also, they indicate the mixed type of the inhibitors adsorption on iron surface. Overall, the AFM measurement demonstrates that **α-APD** and **E-NDPIMA** affects by forming a covering film on the iron surface. Finally, the experimental findings are well correlated with the calculated theoretical parameters. Likewise, molecular dynamics simulations demonstrate that the **α-APD** and **E-NDPIMA** molecules adsorb on the iron surface in a nearby parallel direction.

Appendix A. Supplementary data

Supplementary data related to this article can be found at https://doi.org/10.1016/j.molstruc.2017.12.049.

References

[1] Y.I. Kuznetsov, A.D. Mercer, J.G.N. Thomas, Organic Inhibitors of Corrosion of Metals, Plenum Press, New York, 1996.
[2] C.A. Mann, B.E. Lauer, C.T. Hultin, Organic inhibitors of corrosion, aliphatic amines, Ind. Eng. Chem. 28 (1936) 159–163.
[3] X.H. To, N. Pebere, N. Pelaprat, B. Boutevin, Y. Hervaud, A corrosion-protective film formed on a carbon steel by an organic phosphonate, Corrosion Sci. 39 (1997) 1925–1934.
[4] A.Y. El-Etre, Natural honey as corrosion inhibitor for metals and alloys. I. Copper in neutral aqueous solution, Corrosion Sci. 40 (1998) 1845–1850.
[5] S. Saker, N. Aliouane, H. Hammache, S. Chafaa, G. Bouet, Tetraphosphonic acid as eco-friendly corrosion inhibitor on carbon steel in 3 % NaCl aqueous solution, Ionics 21 (2015) 2079–2090.
[6] M.E. Mashuga, L.O. Olasunkanmi, E.E. Ebenso, Experimental and theoretical investigation of the inhibitory effect of new pyridazine derivatives for the corrosion of mild steel in 1 M HCl, J. Mol. Struct. 1136 (2017) 127–139.
[7] L. Bilgic, N. Caliskan, An investigation of some Schiff bases as corrosion inhibitors for austenite chromium–nickel steel in H_2SO_4, J. Appl. Electrochem. 52 (2001) 79–83.
[8] B. Zhang, C. He, C. Wang, P. Sun, F. Li, Y. Lin, Synergistic corrosion inhibition of environment-friendly inhibitors on the corrosion of carbon steel in soft water, Corrosion Sci. 94 (2015) 6–20.
[9] S.-W. Xie, Z. Liu, G.-C. Han, W. Li, J. Liu, Z. Chen, Molecular dynamics simulation of inhibition mechanism of 3, 5-dibromo salicylaldehyde schiff's base, Comput. Theoret. Chem. 1063 (2015) 50–62.
[10] S.L. Granese, B.M. Rosales, C. Oviedo, J.O. Zerbino, The inhibition action of heterocyclic nitrogen organic compounds on Fe and steel in HCl media, Corrosion Sci. 33 (1992) 1439–1453.
[11] D. Daoud, T. Douadi, S. Issaadi, S. Chafaa, Adsorption and corrosion inhibition of new synthesized thiophene Schiff base on mild steel X52 in HCl and H_2SO_4 solutions, Corrosion Sci. 79 (2014) 50–58.
[12] S. Ramesh, S. Rajeswari, S. Maruthamuthu, Corrosion inhibition of copper by new triazole phosphonate derivatives, Appl. Surf. Sci. 229 (2004) 214–225.
[13] N. Chafai, S. Chafaa, K. Benbouguerra, D. Daoud, A. Hellal, M. Mehri, Synthesis, characterization and the inhibition activity of a new α-aminophosphonic derivative on the corrosion of XC48 carbon steel in 0.5 M H_2SO_4: experimental and theoretical studies, J Taiwan Inst Chem E 70 (2017) 331–344.
[14] H. Amar, J. Benzakour, A. Derja, D. Villemin, B. Moreau, T. Braisaz, Piperidin-1-yl-phosphonic acid and (4-phosphono-piperazin-1-yl) phosphonic acid: a new class of iron corrosion inhibitors in sodium chloride 3% media, Appl. Surf. Sci. 252 (2006) 6162–6172.
[15] V.P. Kukhar, H.R. Hudson, Aminophosphonic and Aminophosphinic Acids, John Wiley & Sons, Chichester, 2000.
[16] X.J. Mu, M.Y. Lei, J.P. Zou, W. Zhang, Microwave-assisted solvent-free and catalyst-free Kabachnik–Fields reactions for α-amino phosphonates, Tetrahedron Lett. 47 (2006) 1125–1127.
[17] K. Moedritzer, R.R. Irani, Synthesis and properties of mono- and polymethylene-diphosphonic acids and esters, J. Inorg. Nucl. Chem. 22 (1961) 297–304.
[18] A. Hellal, S. Chafaa, N. Chafai, L. Touafri, Synthesis, antibacterial screening and DFT studies of series of α-amino-phosphonates derivatives from aminophénols, J. Mol. Struct. 1134 (2017) 217–225.
[19] D. Redmore, Chemistry of phosphorous acid: new routes to phosphonic acids and phosphate esters, J. Org. Chem. 43 (1978) 992–996.
[20] E.K. Fields, The synthesis of esters of substituted amino phosphonic acids, J. Am. Chem. Soc. 74 (1952) 1528–1531.
[21] A. Hellal, S. Chafaa, N. Chafai, Synthesis, characterization and computational studies of three α-amino-phosphonic acids derivatives from Meta, Ortho and Para aminophenol, J. Mol. Struct. 1103 (2016) 110–124.
[22] K. Moedritzer, R.R. Irani, Direct synthesis of α-aminomethylphosphonic acids. Mannich-type reactions with orthophosphorous acid, J. Org. Chem. 31 (1966) 1603–1607.
[23] L. Ouksel, S. Chafaa, R. Bourzami, N. Hamdouni, M. Sebais, N. Chafai, Crystal structure, vibrational, spectral investigation, quantum chemical DFT calculations and thermal behavior of Diethyl [hydroxy (phenyl) methyl] phosphonate, J. Mol. Struct. 1144 (2017) 389–395.
[24] H. Shokry, Molecular dynamics simulation and quantum chemical calculations for the adsorption of some Azo-azomethine derivatives on mild steel, J. Mol. Struct. 1060 (2014) 80–87.
[25] L.O. Olasunkanmi, M.F. Sebona, E.E. Ebenso, Influence of 6-phenyl-3(2H)-pyridazinone and 3-chloro-6-phenylpyrazine on mild steel corrosion in 0.5 M HCl medium: experimental and theoretical studies, J. Mol. Struct. 1149 (2017) 549–559.
[26] M. Messali, H. Lgaz, R. Dassanayake, R. Salghi, S. Jodeh, N. Abidi, O. Hamed, Guar gum as efficient non-toxic inhibitor of carbon steel corrosion in phosphoric acid medium: electrochemical, surface, DFT and MD simulations studies, J. Mol. Struct. 1145 (2017) 43–54.
[27] H.R. Obayes, A.A. Al-Amiery, G.H. Alwan, T.A. Abdullah, A.A.H. Kadhum, A.B. Mohamad, Sulphonamides as corrosion inhibitor: experimental and DFT studies, J. Mol. Struct. 1138 (2017) 27–34.
[28] M.A. Quraishi, R. Sardar, Corrosion inhibition of mild steel in acid solutions by some aromatic oxadiazoles, Mater. Chem. Phys. 78 (2002) 425–431.
[29] H.F. Ma, S.H. Chen, Z.B. Liu, Y.M. Sun, Theoretical elucidation on the inhibition mechanism of pyridine–pyrazole compound: a Hartree Fock study, J. Mol. Struct. 774 (2006) 19–22.
[30] Y.G. Yan, X. Wang, Y. Zhang, P. Wang, X.H. Cao, J. Zhang, Molecular dynamics simulation of corrosive species diffusion in imidazoline inhibitor films with different alkyl chain length, Corrosion Sci. 73 (2013) 123–129.
[31] Z. Tao, S. Zhang, W. Li, B. Hou, Corrosion inhibition of mild steel in acidic solution by oxo-triazole derivatives, Corrosion Sci. 51 (2009) 2588–2595.
[32] M.J. Frisch, G.W. Trucks, H.B. Schlegel, G.E. Scuseria, M.A. Robb, J.R. Cheeseman, G. Scalmani, V. Barone, B. Mennucci, G.A. Petersson, H. Nakatsuji, M. Caricato, X. Li, H.P. Hratchian, A.F. Izmaylov, J. Bloino, G. Zheng, J.L. Sonnenberg, M. Hada, M. Ehara, K. Toyota, R. Fukuda, J. Hasegawa, M. Ishida, T. Nakajima, Y. Honda, O. Kitao, H. Nakai, T. Vreven, J.A. Montgomery Jr., J.E. Peralta, F. Ogliaro, M. Bearpark, J.J. Heyd, E. Brothers, K.N. Kudin, V.N. Staroverov, R. Kobayashi, J. Normand, K. Raghavachari, A. Rendell, J.C. Burant, S.S. Iyengar, J. Tomasi, M. Cossi, N. Rega, J.M. Millam, M. Klene, J.E. Knox, J.B. Cross, V. Bakken, C. Adamo, J. Jaramillo, R. Gomperts, R.E. Stratmann, O. Yazyev, A.J. Austin, R. Cammi, C. Pomelli, J.W. Ochterski, R.L. Martin, K. Morokuma, V.G. Zakrzewski, G.A. Voth, P. Salvador, J.J. Dannenberg, S. Dapprich, A.D. Daniels, O. Farkas, J.B. Foresman, J.V. Ortiz, J. Cioslowski, D.J. Fox, Gaussian 09, Revision A.02, Gaussian, Inc., Wallingford, CT, 2009.
[33] R. Dennington, T.A. Keith, J.M. Millam, GaussView 5.0.8, Semichem Inc., Shawnee Mission, KS, 2009.
[34] R.G. Parr, W. Yang, Density Functional Theory of Atoms and Molecules, Oxford University Press, New York, 1989.
[35] W. Kohn, L.J. Sham, Quantum density oscillations in an inhomogeneous electron gas, Phys. Rev. 137 (1965) 1697–1705.
[36] M. Arivazhagan, V.P. Subhasini, Quantum chemical studies on structure of 2-amino-5-nitropyrimidine, Spectrochim. Acta Part A 91 (2012) 402–410.
[37] M.S. Masoud, A.E. Ali, M.A. Shaker, G.S. Elasala, Synthesis, computational, spectroscopic, thermal and antimicrobial activity studies on some metal–urate complexes, Spectrochim. Acta Part A 90 (2012) 93–108.
[38] V.S. Sastri, J.R. Perumareddi, Molecular orbital theoretical studies of some organic corrosion inhibitors, Corrosion 53 (1997) 617–629.
[39] Materials Studio 7.0, Accelrys Inc., San Diego, CA, 2013.
[40] C. Cao, On electrochemical techniques for interface inhibitor research, Corrosion Sci. 38 (1996) 2073–2082.
[41] P. Raja, M. Sethuraman, Atropine sulphate as corrosion inhibitor for mild steel in sulphuric acid medium, Mater. Lett. 62 (2008) 1602–1604.
[42] Y. Tang, X. Yang, W. Yang, R. Wan, Y. Chen, X. Yin, A preliminary investigationof corrosion inhibition of mild steel in 0.5 M H2SO4by2-amino-5-(n-pyridyl)-1,3,4-thiadiazole: polarization, EIS and molecularmdynamics simulations, Corrosion Sci. 52 (2010) 1801–1808.
[43] F. Bentiss, C. Jama, B. Mernari, H. El Attari, L. El Kadi, M. Lebrini, M. Traisnel, M. Lagrenée, Corrosion control of mild steel using3,5-bis(4-methoxyphenyl)-4-amino-1,2,4-triazole in normal hydrochloricacid medium, Corrosion Sci. 51 (2009) 1628–1635.
[44] N. Labjar, M. Lebrini, F. Bentiss, N.E. Chihib, S. El Hajjaji, C. Jama, Corrosion inhibition of carbon steel and antibacterial properties of aminotris (methylnephosnic) acid, Mater. Chem. Phys. 119 (2010) 330–336.
[45] F. Bentiss, M. Lebrini, M. Lagrenée, Thermodynamic characterization of metal dissolution and inhibitor adsorption processes in mild steel/2,5-bis(n-thienyl)-1,3,4-thiadiazoles/hydrochloric acid system, Corrosion Sci. 47 (2005) 2915–2931.
[46] M. Moradi, J. Duan, X. Du, Investigation of the effect of 4,5-dichloro-2-n-octyl-4-isothiazolin-3-one inhibition on the corrosion of carbon steel in Bacillus sp. Inoculated artificial seawater, Corrosion Sci. 69 (2013) 338–345.
[47] F. Bentiss, M. Lagrenee, M. Traisnel, J.C. Hornez, The corrosion inhibition of mild steel in acidic media by a new triazole derivative, Corrosion Sci. 41 (1999) 789–803.
[48] O.O. Xomet, N.V. Likhanova, M.A.D. Anguilar, E. Arce, H. Dorantes, P.A. Lozada, Synthesis and corrosion inhibition of α-amino acids alkylamides for mild steel in acidic environment, Mater. Chem. Phys. 110 (2008) 344–351.
[49] X. Li, S. Deng, H. Fu, Allyl thiourea as a corrosion inhibitor for cold rolled steel in H_3PO_4 solution, Corrosion Sci. 55 (2012) 280–288.
[50] S. Şafak, B. Duran, A. Yurt, G. Türkoğlu, Schiff bases as corrosion inhibitor for aluminium in HCl solution, Corrosion Sci. 54 (2012) 251–259.

[51] G. Avci, Inhibitor effect of N,N′-methylenediacrylamide on corrosion behavior of mild steel in 0.5 M HCl, Mater. Chem. Phys. 112 (2008) 234–238.
[52] M.J. Bahrami, S.M.A. Hosseini, P. Pilvar, Experimental and theoretical investigation of organic compounds as inhibitors for mild steel corrosion in sulfuric acid medium, Corrosion Sci. 52 (2010) 2793–2803.
[53] M. Behpour, S.M. Ghoreishi, N. Mohammadi, N. Soltani, M. Salavati-Niasari, Investigation of some Schiff base compounds containing disulfide bond as HCl corrosion inhibitors for mild steel, Corrosion Sci. 52 (2010) 4046–4057.
[54] L. Herrag, B. Hammouti, S. Elkadiri, A. Aouniti, C. Jama, H. Vezin, F. Bentiss, Adsorption properties and inhibition of mild steel corrosion in hydrochloric solution by some newly synthesized diamine derivatives: experimental and theoretical investigations, Corrosion Sci. 52 (2010) 3042–3051.
[55] K.F. Khaled, Studies of iron corrosion inhibition using chemical, electrochemical and computer simulation techniques, Electrochim. Acta 55 (2010) 6523–6532.
[56] D. Zhang, Z. An, Q. Pan, L. Gao, G. Zhou, Comparative study of bis-piperidiniummethyl ureaandmono-piperidiniummethyl-ureaas volatile corrosion inhibitors for mild steel, Corrosion Sci. 48 (2006) 1437–1448.
[57] R.M. Issa, M.K. Awad, F.M. Atlam, Quantum chemical studies on the inhibition of corrosion of copper surface by substituted uracils, Appl. Surf. Sci. 255 (2008) 2433–2441.
[58] M. Lashkari, M.R. Arshadi, DFT studies of pyridine corrosion inhibitors in electrical double layer: solvent, substrate, and electric field effects, Chem. Phys. 299 (2004) 131–137.
[59] I. Lukovits, E. Kalman, F. Zucchi, Corrosion inhibitors—correlation between electronic structure and ef- ficiency, Corrosion 57 (2001) 3–8.
[60] S.M. Wetterer, D.J. Lavrich, T. Cummings, S.L. Bernasek, G. Scoles, Energetics and kinetics of the physisorption of hydrocarbons on Au (111), J. Phys. Chem. B 46 (1998) 9266–9275.
[61] S. John, J. Joy, M. Prajila, A. Joseph, Electrochemical, quantum chemical and molecular dynamics studies on the interaction of 4-amino-4H,3,5-di(methoxy)-1,2,4-triazole (ATD), BATD, and DBATD on copper metal in 1N H_2SO_4, Mater. Corros. 62 (2011) 1031–1041.